Gating Ion and Fluid Transport with Chiral Solvent

SCHOLARONE™
Manuscripts

Gating Ion and Fluid Transport with Chiral Solvent

Savannah Silva,[1,#] Siddharth Singh,[2,#] Ethan Cao,[1] John T. Fourkas,[2,3,*] Zuzanna S. Siwy[1,4,5*]

[1]*Department of Physics and Astronomy, University of California, Irvine, CA 92697, USA*

[2]*Department of Chemistry and Biochemistry,* [3]*Institute for Physical Science and Technology, University of Maryland, College Park, Maryland, USA*

[4]*Department of Chemistry,* [5]*Department of Biomedical Engineering, University of California, Irvine, CA 92697, USA*

Abstract: The development of modern membranes for ionic separations and energy-storage devices such as supercapacitors depends on the description of ions at solid interfaces, as is often provided by the electrical double layer (EDL) model. The classical EDL model ignores, however, important factors such as possible spatial organization of solvent at the interface and the influence of the solvent on the spatial dependence of the electrochemical potential; these effects in turn govern electrokinetic phenomena. Here we provide a molecular-level understanding of how solvent structure can dictate ionic distributions at interfaces using a model system of a polar, aprotic solvent, propylene carbonate, in its enantiomerically pure and racemic forms, at a silica interface. We link the interfacial structure to the tuning of ionic and fluid transport by the chirality of the solvent and the salt concentration. The results of nonlinear spectroscopic experiments and electrochemical measurements suggest that the solvent exhibits lipid-bilayer-like interfacial organization, with a structure that is dependent on the solvent chirality. The racemic form creates highly ordered layered structure that dictates local ionic concentrations, such that the effective surface potential becomes positive in a wide range of electrolyte concentrations. The enantiomerically pure form exhibits weaker ordering at the silica surface, which leads to a lower effective surface charge induced by ions partitioning into the layered structure. The surface charge in silicon nitride and polymer pores is probed through the direction of electroosmosis that the surface charges induce. Our findings add a new dimension to the nascent field of chiral electrochemistry, and emphasize the importance of including solvent molecules in descriptions of solid–liquid interfaces.

# These Authors contributed equally

---

* Corresponding Authors: zsiwy@uci.edu, Tel. 714-714-0027; fourkas@umd.edu, 301-405-7996

Introduction

Chirality plays a fundamental role in life. There have been significant efforts made to develop technologies to separate racemic mixtures to create enantiomerically pure samples[1-3] and to perform asymmetric synthesis[4] to provide enantiomerically pure product. Biological channels[5-7] and artificial nanopores[8, 9] have been used to create systems that can distinguish between enantiomeric analytes and to prepare filtration systems capable of transporting a single enantiomer with high selectivity.[10-12] Chiral solvents can also facilitate asymmetric catalysis in some cases.[13]

In this manuscript we consider racemic and enantiomerically pure propylene carbonate (Figure 1A), and ask whether the chiral character of the solvent can affect its organization at solid–liquid interfaces. We probe the influence of the solvent chirality on the effective surface potential of silica–liquid and polymer–liquid interfaces over a range of $LiClO_4$ concentrations. Being an aprotic molecule with a carbonyl group, propylene carbonate (PC) cannot donate hydrogen bonds, but can accept them. Because carbonyl groups are such weak bases, PC cannot induce significant deprotonation of the silanol groups on silica, as suggested by the high pK_a values of acids in this and other aprotic solvents.[14, 15] Yet a PC molecule features a dipole moment of 4.9 D. Interestingly, the racemic form of this solvent has been shown to induce an effective positive potential at the solid–liquid interface in polymer and glass nanopores.[16, 17] The origin of the positive potential was hypothesized to stem from adsorption of lithium ions, as well as from organization of the solvent molecules at the interface.[18] If the solvent organization is indeed responsible for the finite effective potential of silica and polymers in PC, then the interfacial molecular arrangement and effective potential are expected to be sensitive to whether the solvent is racemic or enantiomerically pure. Consequently, porous media could exhibit different ionic and fluidic transport for the same concentration of electrolyte but different forms of the solvent. Note that interfacial layering of the solvent could determine the effective surface potential through local charges of the dipole molecules, and can also affect the locations of ions within and outside of the layers.[18]

To probe the interfacial organization of PC, as well as the presence and polarity of an effective surface potential on silica, we combined two experimental approaches. First, we used vibrational sum-frequency-generation spectroscopy (VSFG)[19, 20] to determine the molecular organization of racemic and enantiomerically pure PC at the silica–liquid interface. Next, electrokinetic experiments were performed to determine the effective potential of the silica and polymer interfaces. [19] To this end, electroosmosis was measured as a function of $LiClO_4$ concentration in pores in both silicon nitride and polymers. We note that a similar approach has been recently

applied to probe solid–liquid interface of silica with acetonitrile-based electrolyte solutions.[18] Acetonitrile is also characterized by a high dipole moment, 3.9 D, and was found to create a highly organized, lipid-bilayer-like (LBL) structure in which the cyano groups accept hydrogen bonds from the silica silanol groups.[21] The spatial organization of acetonitrile was preserved even in 1 M $LiClO_4$, and governed the locations of the cations and anions at all concentrations studied.[18] In this manuscript we show that PC also creates a spatially organized structure at silica and polymer interfaces that is sensitive to the chirality of the solvent. Electroosmosis measured in salt gradients allows us to conclude that it is the solvent organization that primarily influences ionic and fluidic transport, in contrast to the predictions of EDL theory.

Materials and Methods

Chemicals

Lithium perchlorate ($LiClO_4$, ≥99.99% battery grade, Sigma Aldrich), racemic propylene carbonate (Sigma Aldrich with 99.7% pure HPLC Grade), and the R and S enantiomers of propylene carbonate (TCI chemicals, purity >98%) were used in the experiments. The PC was stored in a glovebox, and small amounts of the solvents were taken out to prepare solutions that were used within a few hours.

VSFG experiments

VSFG experiments were performed as described previously (Figure 1B,C).[22] Briefly, in the VSFG spectrometer setup, a Ti:sapphire oscillator (Mira Basic, Coherent) is used to seed a regenerative amplifier (Legend Elite, Coherent). The amplifier generates pulses of 800 nm with a pulse duration of 80 fs and repetition rate of 1 kHz. The amplifier output has an average power of 3 W, 1 W of which is directed into an OPA/DFG module (TOPAS, Light Conversion) to produce an IR beam with a bandwidth of 250 cm^{-1} centered at 2945 cm^{-1} and a maximum pulse energy of 15 µJ. This IR beam excites vibrations in the C–H stretching region of the infrared spectrum. The remaining power of the amplifier output is spectrally narrowed with a slit in a *4f* pulse stretcher, sent through a delay stage, and then focused on the sample. The slit reduces the bandwidth to 5 cm^{-1}. The 800-nm probe beam has a power of 15 µJ. The IR and probe beams meet at the sample in a counter-propagating geometry. The probe and IR beams are incident at 61° and −58° from the surface normal, respectively. The signal is generated at a −32.8° angle, and is collected using a spectrometer (ActonSP300i) with a thermoelectrically cooled CCD camera (Spec-10:100, Roper Scientific). The experiments were performed in the SSP, PPP and SPS polarization configurations, with the polarizations listed in the order of the signal, probe, and IR beams. P

denotes polarization parallel to the surface normal, and S denotes polarization perpendicular to the surface normal. Eight, 120-s scans were performed for each sample.
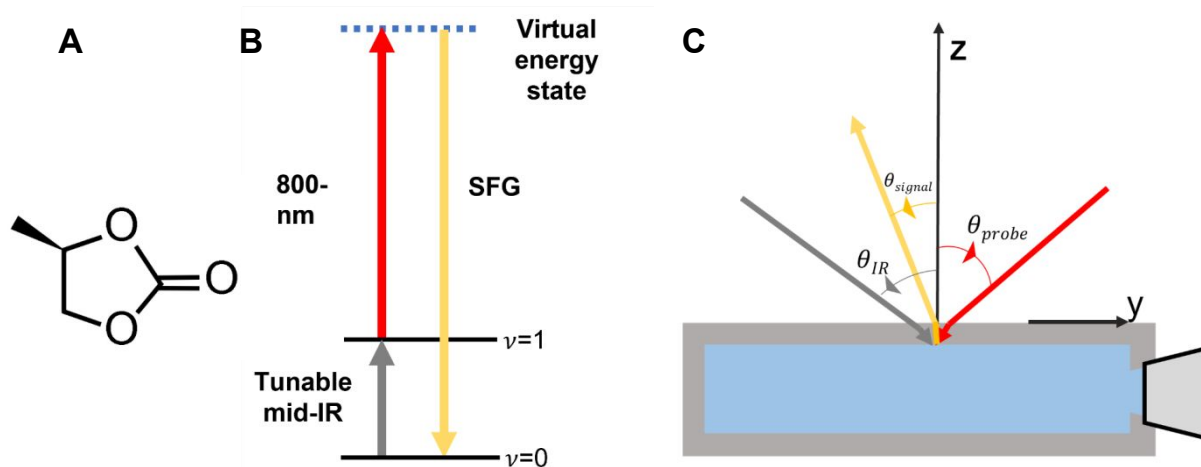

Figure 1. *The VSFG spectroscopy scheme used to obtain results presented in this manuscript. (A) The chemical structure of R-(+)-propylene carbonate. (B) A Jablonski diagram of the VSFG process. An IR pump beam excites a vibration that is IR active. The vibration is then probed via a Raman transition through a virtual state, which is driven by an 800-nm laser, generating a signal at the sum of the two frequencies. (C) A schematic of the counter-propagating VSFG geometry used to obtain the data in this paper. The IR and probe beams approach an IR quartz cuvette filled with the solvent from opposite directions, yielding a signal that propagates in a unique direction.*

The individual spectra were normalized to the nonresonant SFG signal of a gold substrate. A polystyrene film placed in the path of the IR beam while measuring the gold SFG signal was used for frequency calibration of the signal, using four polystyrene absorption peaks. The cleaning process before use of the cuvettes involved rinsing with contaminant-free acetone, methanol, and then water. The cuvettes were then oven-dried, and cleaned for 3 min in an oxygen plasma.

Pore preparation

Two types of pores were used in measurements: single nanopores in 20-nm-thick silicon nitride, and single pores in 12-μm-thick polyethylene terephthalate (PET). Silicon nitride pores were purchased from Norcada, and had an opening diameter of 30 nm.

Single polymer pores in PET films were prepared using the track-etching technique, which entails irradiation of the films with a single, energetic heavy ion (UNILAC at the Institute for Heavy Ions Research in Darmstadt, Germany), and subsequently etching in 2 M NaOH at 50 °C.[23, 24] These etching conditions have been shown previously to lead to the formation of symmetric pores. The diameters of these single pores were estimated by assuming that the pores were filled with bulk solution and that the pore shape was cylindrical. Sizing of all pores was performed in an aqueous solution of 1 M KCl. Experiments with pores of diameters 370 nm and 450 nm are presented in this paper. The PET films had a circular shape with a 3 cm diameter, and the single pore was located within a 100-μm-diameter circle in the middle that was the location of the opening of a metal mask that restricted access of the heavy ions to this region. This relatively small area exposed to the heavy ions in a defocused beam enables one to restrict the number of ions passing through to one.[25] Consequently, all such membranes used in this study contained only one pore.

Ion-current measurements

Electrokinetic characterization of single pores was performed in a home-made conductivity cell in which a single-pore membrane separated two chambers of a conductivity cell. Two different designs of the conductivity cell were used to accommodate the larger PET films and the smaller TEM chips. Each membrane was exposed to a concentration gradient of $LiClO_4$ prepared with either in racemic or enantiomerically pure PC. The concentration gradients used were 0.1 mM/1 mM, 0.5 mM/5 mM, 1 mM/10 mM, and 10 mM/100 mM. Current–voltage curves were recorded using Keithley 6487 picoammeter/voltage source (Keithley Instruments, Cleveland, OH) and two pellet Ag/AgCl electrodes. The voltage was varied between -2 V and +2 V with 0.1 V steps. All current–voltage curves show average values and standard deviations from at least three scans. Before switching salt concentration, both chambers of the conductivity cell were soaked thoroughly in neat PC.

Results and Discussion

VSFG spectra of racemic and enantiomeric propylene carbonate

To probe whether PC forms a spatially organized structure on the silica surface, VSFG measurements were performed on a flat IR quartz substrate in contact with racemic or enantiomerically pure PC. VSFG is uniquely sensitive to the arrangement of molecules at

interfaces between isotropic media, where symmetry is broken, because within the electric dipole approximation the VSFG signal of an isotropic or centrosymmetric medium is zero.[26] The polarization configuration that we measure is described in terms of the signal polarization, the 800-nm probe polarization, and the tunable IR pump polarization. Each polarization combination has a different sensitivity to the orientations of the IR transition dipoles, and hence can provide information on the orientation of the molecules at the interface. The SSP polarization configuration is most sensitive to IR transition dipoles that have a significant projection along the surface normal, the SPS polarization configuration is most sensitive to IR transition dipoles that have a significant projection along the surface, and the PPP polarization configuration is sensitive to IR transition dipoles with a significant projection in either of these directions.

Figure 2A shows VSFG signals for racemic PC in all three polarization configurations in the C-H stretching region. PC has a methyl group, and methylene group, and a methine group. The former two groups have both symmetric and asymmetric stretches. All of the C-H stretching modes are both IR and Raman active, and so should appear in the VSFG spectrum. The modes for individual groups cannot be distinguished in these spectra. The likely causes for the broad peaks include spectral overlap, the existence of two nearly isoenergetic conformers (with the methyl group axial and equatorial, respectively), possible mode mixing, and the potential presence of Fermi resonances. The two broad peaks that we observe can generally be attributed, however, to symmetric C-H stretches ($\sim$2920 cm^{-1}) and asymmetric C-H stretches ($\sim$2980 cm^{-1}) The SSP signal is considerably stronger than the SPS or PPP signals, which we attribute to unfavorable nonlinear Fresnel factors for the latter two polarization configurations. In all cases the peak for the asymmetric stretches is stronger than that for the symmetric stretches. The prominence of the asymmetric stretches in the SSP spectrum suggests that the methyl and methylene groups have a substantial projection parallel to the surface. The fact that the symmetric stretch signal is somewhat stronger in relation to the asymmetric stretch signal in the other polarization configurations supports this picture. The symmetric stretch peak likely remains weaker than the asymmetric stretch peak under SPS and PPP conditions because symmetric C-H stretches are generally strongly polarized, whereas asymmetric stretches are depolarized.

It is useful to begin by revisiting the VSFG spectra and molecular organization of acetonitrile at a silica interface. The first sublayer of the acetonitrile LBL structure at the interface is composed largely of molecules that accept hydrogen bonds from surface silanol groups.[21] Due to inductive effects, this hydrogen bonding leads to a shift in the symmetric methyl stretching frequency compared to that of the molecules in the second sublayer, which do not accept hydrogen bonds.

This shift causes acetonitrile to have a strong VSFG signal for the symmetric methyl stretch at this interface.

The carbonyl group of PC is also expected to accept hydrogen bonds from surface silanol groups. However, because there are no hydrogen atoms bonded to the carbons that are adjacent to the carbonyl group (Figure 1A), any inductive effects in the C-H stretching frequencies are expected to be minimal. The weak VSFG signal for PC at this interface is therefore suggestive of the formation of a relatively centrosymmetric surface organization. Although PC is not a linear molecule, and therefore is not a traditional amphiphile, a PC molecule does feature distinct halves, one of which is strongly polar and the other of which is hydrophobic.[27] Furthermore, it is expected to be energetically favored for the PC molecules nearest to the silica surface to accept hydrogen bonds from silanol groups, therefore presenting the hydrophobic region of the molecules to the bulk liquid. This hydrophobic layer will further favor interactions with PC molecules that point in the opposite direction, creating a roughly centrosymmetric structure. Given that the molecules that accept hydrogen bonds from silanol groups must be relatively well ordered, our VSFG results suggest that PC, like acetonitrile, takes on an LBL organization at the silica–liquid interface. This picture is also supported by previous molecular dynamics simulations of the organization of PC molecules on a positively-charged graphite electrode that revealed the formation of an LBL structure, with the carbonyl oxygens pointing towards the electrode.[28] As discussed below, electrochemical measurements additionally support the idea that PC forms an LBL interfacial organization.

Figure 2B compares VSFG spectra in the SSP polarization configuration for racemic and both forms of enantiomerically pure (R and S) PC. The spectra for the two enantiomers are comparable. However, both peaks are considerably stronger for the enantiomerically pure liquids than for the racemic liquid, although the signal is still considerably smaller than that for acetonitrile at the same interface. Furthermore, the symmetric and asymmetric stretch peaks are of comparable heights for the enantiomerically pure liquids. The stronger VSFG signal for the enantiomerically pure PC suggests that a single enantiomer cannot form an LBL structure that is as well organized as that formed in the racemic liquid, leading to a reduced cancellation of signals from molecules pointing in opposite directions at the interface. However, the VSFG signal is still relatively weak for the enantiomerically pure liquids, suggesting that an LBL structure does still persist. The enhancement of the symmetric stretch signal further suggests that the methyl and methylene groups may have a greater projection along the surface normal in the enantiomerically pure liquid. Finally, we note that the stronger signal in the enantiomerically pure liquids does not

appear to arise from the lack of inversion symmetry based on having a single enantiomer, as no VSFG signal was observed under SPP polarization conditions, in which a signal can only be observed in a chiral system.
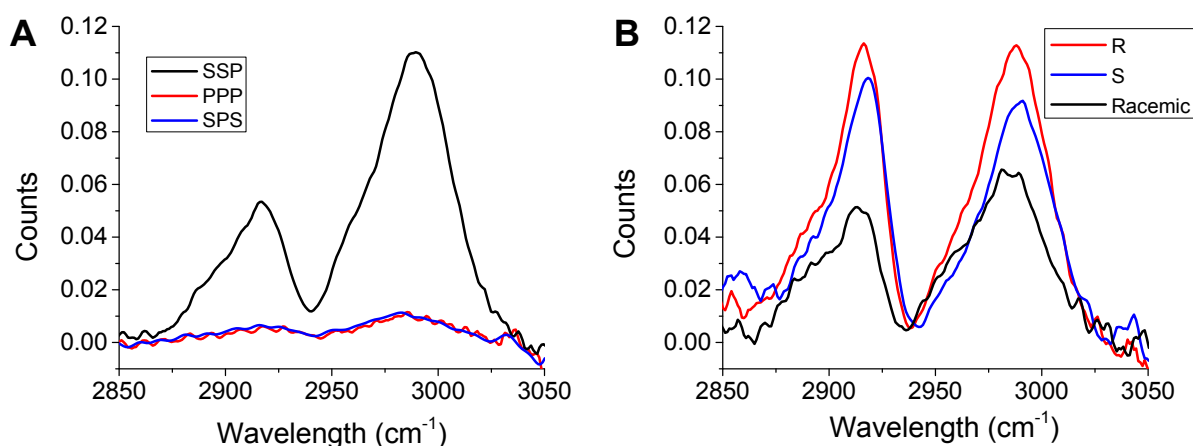

Figure 2. *(A) VSFG spectra of neat racemic propylene carbonate at silica interface at three configurations of the transitional dipoles. (B) SSP VSFG spectra of racemic and enantiomerically pure R and S PC at a silica interface.*

Electroosmosis in LiClO$_4$ solutions in enantiomerically pure and racemic PC.

Our VSFG measurements suggest that enantiomerically pure and racemic samples of PC both exhibit spatial organization at a silica interface. As a next step, we probed the consequences of the interfacial structure for ionic and fluidic flow. Specifically, we sought to determine whether electroosmosis in PC is sensitive enough to detect differences in the interfacial organization of the racemic and enantiomerically pure liquids that were revealed by VSFG.
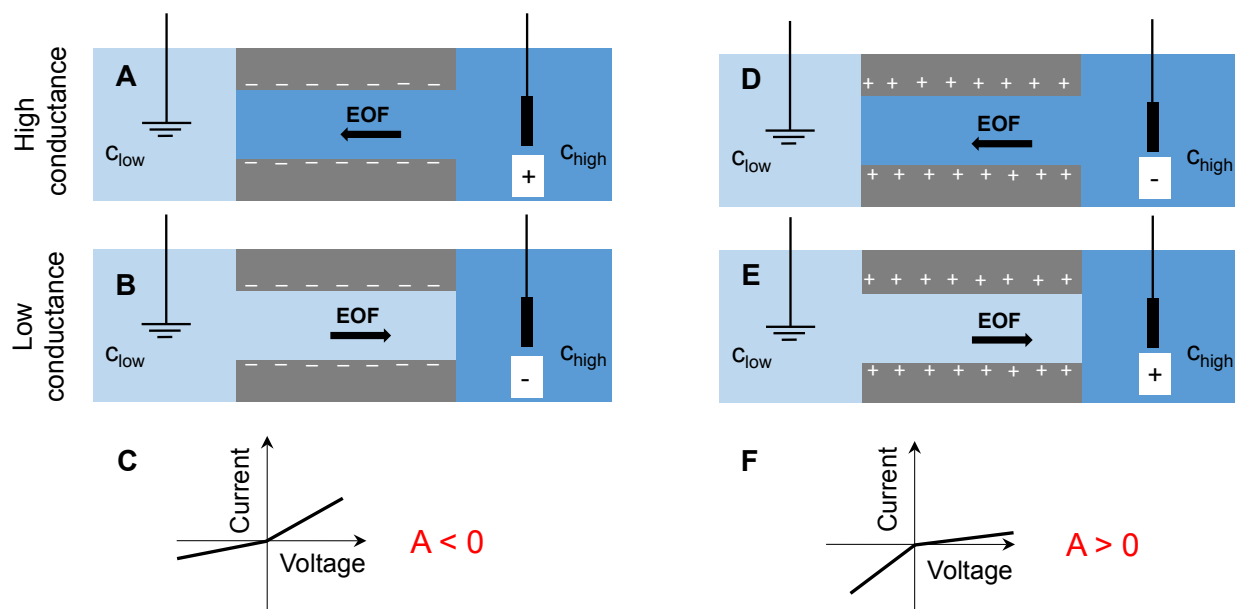
Figure 3. *Schematic of electroosmotically-driven ion-current rectification. (A-F) A single pore is in contact with a salt-concentration gradient. The ground electrode is placed in the solution with the lower salt concentration, c_{low}, indicated in a lighter shade of blue. The arrows in A, B, D and E indicate the direction of electroosmosis determined by the migration of counterions. (A) A pore with a negative effective surface potential will be filled with the more concentrated solution, c_{high}, indicated in darker blue, for positive transmembrane potentials when the direction of electroosmosis is from c_{high} to c_{low}. (B) The same pore will be filled with the less concentrated solution, c_{low}, for negative voltages. (C) Having more ions in the pore at positive voltages will lead to higher positive currents than negative currents, resulting in rectifying current–voltage curves. (D) A pore with a positive surface potential will be filled with the more concentrated solution for negative voltages, because in this case the direction of electroosmosis is determined by the migration of anions. (E) Positive voltages will fill the pore with c_{low}. (F) Consequently, in the current–voltage curve, the negative currents are larger than the positive currents. The parameter A is the ion-current anisotropy, as defined in eq. (1).*

Figure 3 shows a schematic of our experimental setup, in which a single pore is placed in contact with a salt concentration gradient. The presence of different salt concentrations, c_{high} and c_{low}, on each side of the membrane naturally leads to ion-current rectification, but only when the interface exhibits a non-zero potential.[24] If the ground electrode is located in the less concentrated solution and the interface carries an effective negative potential, the direction of electroosmosis will be

determined by the cations, which will electroosmotically drag the more concentrated solution, c_{high}, into the pore at positive voltages (Figure 3A). When a negative voltage is applied, again keeping the ground in the less concentrated solution, a pore with negative potential will be filled with the solution of lower concentration, c_{low} (Figure 3B). Consequently, an asymmetric current–voltage curve will be recorded, such that $|I(+V)| > |I(-V)|$ (Figure 3C). On the other hand, if the pore carries an effective positive potential, the direction of electroosmosis will be determined by the anions. Such a pore will be filled with the more concentrated solution, c_{high}, for negative voltages, whereas positive voltages will bring c_{low} into the pore. A pore with positive surface potential will also exhibit asymmetric current–voltage (I–V) curves with $|I(+V)| < |I(-V)|$ (Figure 3F). Pores with negative and positive surface potentials can thus be distinguished easily from the character of their I–V curves recorded under the salt-concentration gradient.

The level of asymmetry of the I–V curves provides an indirect measure of the magnitude of the effective surface potential. For high surface potentials, electroosmosis can fill the entire volume of the pore with a solution of either lower or higher concentration.[24] Consequently, the ratio of currents measured at positive and negative voltages will be equal to the ratio of the ionic conductivities of the solutions. If, on the other hand, the surface potential allows only a part of the pore volume to be filled with solution on either side, the observed asymmetry will be lower. All I–V curves were characterized by the ion-current anisotropy, A, which is defined as:[18]

$$A(V) = \frac{I(-V) + I(V)}{I(-V) - I(V)} \qquad \text{eq. (1)}$$

In our electrode configuration, A assumes positive values when a pore has a positive effective potential, and negative values when the interface has negative effective potential. The sign and magnitude of the parameter A facilitate comparison of effective surface potentials measured under different conditions. However, in order to relate this parameter to the magnitude of the effective surface potential, it would be necessary to perform additional measurements, such as polarimetric angle-resolved second-harmonic scattering[29] or streaming current,[30] as well as to do modeling.
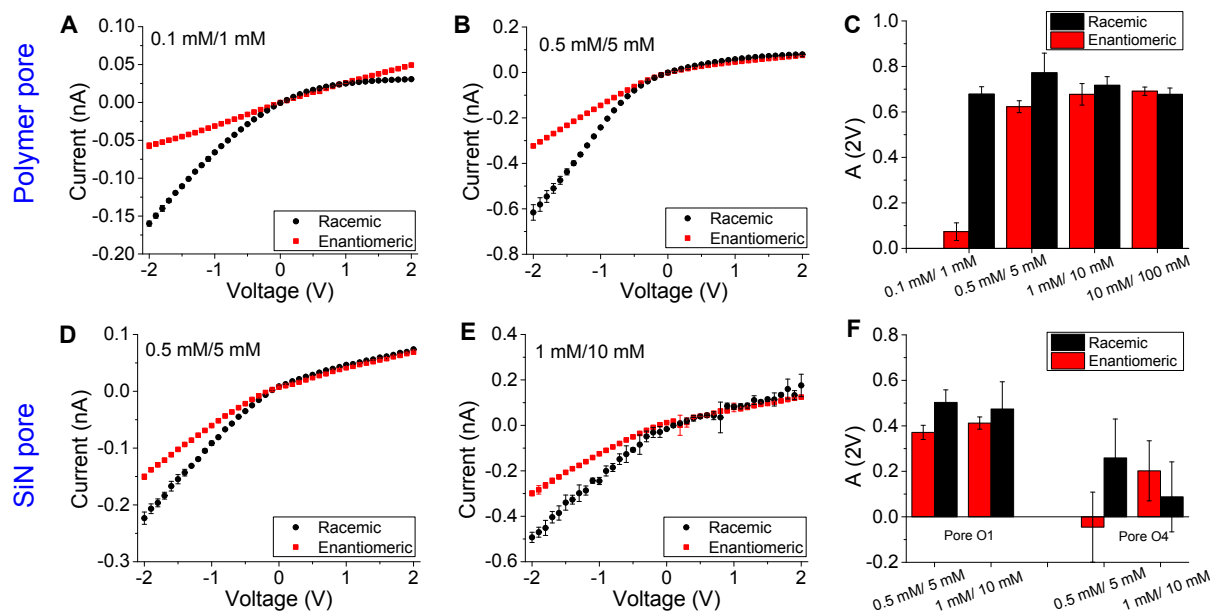
Figure 4. *I–V data for a single, 450-nm-diameter PET pore (A-C) and a single, 30-nm-diameter silicon nitride pore (D-F), each including a summary of the current anisotropy A(2V), as defined in eq. (1). The bar graph in (F) shows A(2V) for two independent pores, O1 and O4. (A) and (B) contain recordings at the LiClO$_4$ concentration gradients of 0.1 mM/1 mM and 0.5 mM/5 mM, respectively. (D) and (E) show recordings at the gradients of 0.5 mM/5 mM and 1 mM/10 mM.*

Figure 4 shows representative I–V curves and *A*(2V) for a single PET pore with diameter of 450 nm and a single silicon nitride pore with an opening of 30 nm. Recordings were performed with solutions prepared using racemic PC and solutions prepared with enantiomerically pure R-PC. When the PET pore was in contact with the lowest concentration gradient, 0.1 mM and 1 mM LiClO$_4$, the I–V curves in the racemic solutions suggested that this pore had effective positive potential (black points in Figure 4A). Yet, the same pore in the same concentration gradient prepared using the enantiomerically pure PC exhibited a nearly linear I–V curve, indicating that the effective surface potential was close to zero (red points in Figure 4A). When the concentration on both sides of the pore was increased by a factor of five (Figure 4B), the pore rectified in the same direction in both racemic and enantiomerically pure PC, but the ion-current anisotropy was again higher in the racemic case. As the ion concentrations were increased further, the I–V curves and values of *A*(2V) for both types of solutions became identical (Figure 4C). A set of data for an independently prepared pore with an opening of 370 nm is shown in the Supplementary Information file, Figure S1.

The data for the silicon nitride nanopores (Figure 4 D-F) were more difficult to record due to the challenges of 'wetting' the 30-nm-diameter pore with PC, which is viscous at room temperature. We chose pores with this diameter based on the thinness of the silicon nitride films. To induce electroosmosis-based rectification in a salt-concentration gradient, the pore must have a finite aspect ratio, such that the transport properties are influenced by the ionic concentration in the pore, and not only by the pore mouth in the region of access resistance.[31] Similar to the experiments in PET pores, however, ion-current data in racemic 0.5 mM/ 5 mM solutions indicated that the surface potential was positive (Figure 4D). The current values at the lowest pair of concentrations, 0.1 mM/1 mM, were unstable for some pores, and so we do not report values of A(2V) for this gradient. Current–voltage curves in enantiomerically pure solutions, in general, also exhibited less ion-current rectification than in racemic PC (Figure 4 E,F), similar to the data for the PET pores. Figure 4 D-F shows recordings for one 30-nm-diameter SiN pore (designated as O1). Values of A(2V) for another SiN pore (O4) are also shown in Figure 4F. Due to the difficulties with the pore wetting, we report recordings in only two concentration gradients.

Recording I–V curves in SiN pores was also challenging, because in some cases the recorded currents in the same concentration gradient of LiClO$_4$ were significantly different in racemic and enantiomerically pure solutions for both voltage polarities, suggesting that the pores had different resistances (Figure S2). We have not yet determined the explanation for this effect, because the salt concentration in all solutions was carefully controlled, and the ionic conductivity of the enantiomerically pure and racemic solutions is expected to be the same.[32] Figure 4D-F was, however, created based on recordings in which the pore conductances in the linear I–V regime were the same at a given concentration gradient in racemic and enantiomerically pure solutions, as seen in PET pores. The identical conductances in the linear regime give us confidence that we have captured nonlinear effects that stem from different effective surface potentials.

The positive effective potential in the presence of LiClO$_4$ solutions in PC was observed in multiple SiN and polymer pores. Because all silicon nitride pores were incubated in piranha solution prior to use, the surface silanol groups produced by this treatment create a surface that is similar in its chemical properties to that of the quartz surface used in VSFG experiments. The PET surface, on the other hand, contains carboxyl groups at a density of up to 1 per nm^2.[33] We postulate that the effective positive potential of the solid–liquid interface originates from the interfacial organization of the solvent in both silica–liquid and polymer–liquid interfaces that dictates the interfacial ionic distributions, as we have found previously for acetonitrile.[18]

It is important to note that some of the pores studied here exhibited a positive effective potential even in the gradient with the lowest concentrations, 0.1 mM/1 mM. On the other hand, glass pores in contact with 0.1 mM/1 mM $LiClO_4$ solutions in acetonitrile exhibited a negative effective potential at low electrolyte concentrations, which we attributed to the organized layer of the solvent molecules and unscreened partial negative charges on nitrogen.[18] Only in the gradient of 1 mM/10 mM in acetonitrile did the glass pores exhibit an effective positive surface potential. The observation of positive potential in a wider range of $LiClO_4$ concentrations in PC than in acetonitrile points to the possibility of lithium ions partitioning into the surface bilayer at lower concentrations in PC, suggesting that the surface LBL organization in PC is less thermodynamically stable and/or more disordered than that in acetonitrile.

Finally, we consider the source of the lower positive potential in solutions of the enatiomerically pure solvent. Insights into the molecular organization at the interface can be gleaned from our VSFG spectra (Figure 2). The racemic PC creates a more centrosymmetric system, with the solvent molecules being more ordered in the surface bilayer as compared to the enantiomerically pure system. Consequently, the LBL organization in racemic solutions will impose different partition coefficients for cations and anions in the bilayer, and will dictate the locations of both types of ions in a concentration-dependent manner.[18] Lithium will first accumulate at the exterior of the bilayer, and will be more likely to enter the bilayer due to the partial negative charges on the oxygen atoms. The interface can then become positively charged even at relatively low $LiClO_4$ concentrations. We expect that with the addition of more concentrated solutions in the racemic liquid, the partition of cations and anions to LBL becomes less restricted, similar to what was observed for acetonitrile. We note also that the nitrogen atom in the cyano group in acetonitrile[34] has a similar charge to the carbonyl oxygen in PC.[35]

Enantiomerically pure PC exhibits a more disordered bilayer than does racemic PC, which intrinsically creates a weaker surface potential in the neat liquid. We postulate that the combination of these effects makes it thermodynamically favorable for both cations and anions to enter the bilayer, lowering the effective positive potential. With the increase of the salt concentration, the layers in the racemic and enantiomerically pure solvents may have a similar influence on the partitioning of ions, leading to comparable values of $A(2V)$.

Conclusions

Combined VSFG and electrokinetic measurements have revealed that propylene carbonate creates an interfacial structure whose details are sensitive to the chirality of the solvent. At the

silica and polymer interfaces, racemic propylene carbonate creates a layered structure that is more ordered than that of enantiomerically pure PC. Results for both types of PC are, however, in strong contrast to the classic picture of the electrical double-layer, in which the solvent is treated as a homogenous continuum. Our results also point to the potential for tuning ionic and fluidic transport with solvent chirality. Chirality-controlled transport is a consequence of chirality influencing the molecular organization of the interface, and thereby the effective surface potential. The greater access of ions to the surface afforded by enantiomerically pure PC may have practical uses in applications such as batteries and supercapacitors.

Conflicts of interest

There are no conflicts to declare.

Acknowledgements

References

1. Y. Okamoto and T. Ikai, *Chem. Soc. Rev.*, 2008, **37**, 2593-2608.
2. Q. Cheng, Q. Ma, H. Pei and Z. Mo, *Sep. Purif. Technol.*, 2022, **292**, 121034.
3. M. Ciriani, R. Oliveira and C. A. M. Afonso, *Green Chem.*, 2022, **24**, 4328-4362.
4. E. M. Carreira and L. Kvaerno, *Classics in Stereoselective Synthesis*, Wiley-VCH, Weinheim; 2009.
5. J. A. Cooper, S. Borsley, P. J. Lusby and S. L. Cockroft, *Chem. Sci.*, 2017, **8**, 5005-5009.
6. A. J. Boersma and H. Bayley, *Angew. Chem. Int. Ed.*, 2012, **51**, 9606-9609.
7. J. Wang, J. D. Prajapati, F. Gao, Y.-L. Ying, U. Kleinekathöfer, M. Winterhalter and Y.-T. Long, *J. Am. Chem. Soc.*, 2022, **144**, 15072-15078.
8. F. Zhang, Y. Sun, D. Tian and H. Li, *Angew. Chem. Int. Ed.*, 2017, **56**, 7186-7190.
9. C. Han, X. Hou, H. Zhang, W. Guo, H. Li and L. Jiang, *J. Am. Chem. Soc.*, 2011, **133**, 7644-7647.
10. Z. Sun, J. Hou, L. Li and Z. Tang, *Coord. Chem. Rev.*, 2020, **425**, 213481.
11. B. B. Lakshmi and C. R. Martin, *Nature*, 1997, **388**, 758-760.
12. S. B. Lee, D. T. Mitchell, L. Trofin, T. K. Nevanen, H. Söderlund and C. R. Martin, *Science*, 2002, **296**, 2198-2200.
13. Y. Nagata, R. Takeda and M. Suginome, *ACS Cent. Sci.*, 2019, **5**, 1235-1240.

14.   K. Izutsu, I. M. Kolthoff, T. Fujinaga, M. Hattori and M. K. Chantooni, *Anal. Chem.*, 1977, **49**, 503-508.
15.   E. Rossini and E.-W. Knapp, *J. Comput. Chem.*, 2016, **37**, 1082-1091.
16.   T. Plett, W. Q. Shi, Y. H. Zeng, W. Mann, I. Vlassiouk, L. A. Baker and Z. S. Siwy, *Nanoscale*, 2015, **7**, 19080-19091.
17.   R. A. Lucas, C.-Y. Lin and Z. S. Siwy, *J. Phys. Chem. B*, 2019, **123**, 6123-6131.
18.   J. W. Polster, A. J. Souna, M. H. Motevaselian, R. A. Lucas, J. D. Tran, Z. S. Siwy, N. R. Aluru and J. T. Fourkas, *Nat. Sci.*, **2**, e20210099.
19.   M. Buck and M. Himmelhaus, *J. Vac. Sci. Technol. A*, 2001, **19**, 2717-2736.
20.   F. Vidal and A. Tadjeddine, *Rep. Prog. Phys.*, 2005, **68**, 1095.
21.   B. J. Berne, J. T. Fourkas, R. A. Walker and J. D. Weeks, *Acc. Chem. Res.*, 2016, **49**, 1605-1613.
22.   F. Ding, Z. Hu, Q. Zhong, K. Manfred, R. R. Gattass, M. R. Brindza, J. T. Fourkas, R. A. Walker and J. D. Weeks, *J. Phys. Chem. C*, 2010, **114**, 17651-17659.
23.   S. Müller, C. Schötz, O. Picht, W. Sigle, P. Kopold, M. Rauber, I. Alber, R. Neumann and M. E. Toimil-Molares, *Cryst. Growth Des.*, 2012, **12**, 615-621.
24.   Y. H. Qiu, R. A. Lucas and Z. S. Siwy, *J. Phys. Chem. Lett.*, 2017, **8**, 3846-3852.
25.   R. Spohr, Method and device to generate a predetermined number of ion tracks, German Patent DE 2 951 376 C2 (issued 15.09.1983); United States Patent No. 4 369 370, 1983.
26.   P. N. Butcher and D. Cotter, *The Elements of Nonlinear Optics*, Cambridge University Press, 1990.
27.   X. You, M. I. Chaudhari, L. R. Pratt, N. Pesika, K. M. Aritakula and S. W. Rick, *J. Chem. Phys.*, 2013, **138**, 114708.
28.   L. Yang, B. H. Fishbine, A. Migliori and L. R. Pratt, *J. Chem. Phys.*, 2010, **132**, 044701.
29.   M. Bischoff, D. Biriukov, M. Předota, S. Roke and A. Marchioro, *J. Phys. Chem. C*, 2020, **124**, 10961-10974.
30.   R. B. Schoch, J. Y. Han and P. Renaud, *Rev. Mod. Phys.*, 2008, **80**, 839-883.
31.   C. Lee, L. Joly, A. Siria, A.-L. Biance, R. Fulcrand and L. Bocquet, *Nano Lett.*, 2012, **12**, 4037-4044.
32.   P. Jankowski, K. Grzegorzewska, A. Szabłowska, M. Piszcz, M. Dranka, G. Z. Żukowska and M. Kalita, *Electrochim. Acta*, 2015, **175**, 240-246.
33.   A. Wolf, N. Reber, P. Y. Apel, B. E. Fischer and R. Spohr, *Nucl. Instrum. Methods Phys.*, 1995, **105**, 291-293.
34.   A. M. Nikitin and A. P. Lyubartsev, *J. Comput. Chem.*, 2007, **28**, 2020-2026.
35.   M. I. Chaudhari, J. R. Nair, L. R. Pratt, F. A. Soto, P. B. Balbuena and S. B. Rempe, *J. Chem. Theory Comput.*, 2016, **12**, 5709-5718.